High Cycle Fatigue Properties and Fracture Behavior of TC4 Titanium Alloy at Room and Elevated Temperatures

Juan Li[1(✉)], Jianming Cai[1], Min Zhou[2], Rui Duan[1], and Xu Huang[1]

[1] AECC Beijing Institute of Aeronautical Materials, Beijing 100095, China
lervly@sina.com
[2] Wuxi Hyatech Co., Ltd, Wuxi 214142, China

Abstract. The high cycle fatigue properties and fracture characteristics of TC4 titanium alloy at room temperature, 200 °C and 400 °C under the stress concentration factors $K_t = 1$ and $K_t = 3$ were studied. The *S-N* curves of rotary bending fatigue under different conditions were plotted by power function fitting of three parameters, and the fatigue limit of $N_f = 3 \times 10^7$ cycles was obtained. The results indicated that TC4 alloy had a high fatigue notch sensitivity at both room and elevated temperatures, which led to the significant decline of fatigue properties. It was found that the smooth specimen was more sensitive to the effect of temperature, whose high cycle fatigue performance decreased obviously with the increase of temperature. There was only one fatigue crack source region in the smooth specimen, and obvious fatigue bands and a small number of secondary cracks can be seen in the propagation region. With the propagation of cracks, instantaneous fracture occurred in the inner side of the specimen opposite the source region. Multiple fatigue crack sources were formed on the surface of the notched specimen, and then the fatigue cracks expanded from the circumference inward. Finally, instantaneous fracture occurred in the inner part of the specimen. TC4 alloy was characterized by ductile fatigue fracture.

Keywords: TC4 titanium alloy · Stress concentration factor · Temperature · High cycle fatigue · Fatigue fracture morphology

1 Introduction

Due to the excellent characteristics of low density, high specific strength, high temperature resistance and corrosion resistance, titanium alloys have been widely used in the fields of aerospace, automobile, ship, petrochemical, biomedical and marine engineering [1–3]. Among all the Ti alloys, TC4 alloy with the nominal composition of Ti–6Al–4V (wt.%) has the largest usage in the aviation industry at present [4–6]. This alloy is a typical $\alpha + \beta$ dual phase alloy, which exhibits both the advantages of α phase and β phase, and has good comprehensive mechanical properties, plasticity, weldability and corrosion resistance. The long-term service temperature of TC4 alloy can reach to

Chinese Society of Aeronautics and Astronautics: CASTYSF 2022, LNEE 972, pp. 278–286, 2023.
https://doi.org/10.1007/978-981-19-7652-0_26

350 °C. Therefore, it is often used in aero-engine discs, blades and other components as a high-temperature titanium alloy [7, 8].

The rotating parts of aero-engine are subjected to complex alternating loads during service. Under complex service conditions, fatigue failure is one of the main reasons for material fracture [9]. A large number of fatigue failure events of aero-engine turbines, rotors and blades show that the main failure causes are torsional and bending resonance fatigue. Among them, the accident rate caused by high cycle fatigue damage is as high as 24%, which is the largest among all accident causes [10, 11]. The high-cycle fatigue properties of Ti alloys are closely related to the service temperature and microstructure. In addition, since the fatigue properties of Ti alloys are sensitive to notches, the stress concentration factor also has a significant impact on its high-cycle fatigue properties [12–14].

At present, the research on high cycle fatigue of TC4 alloy mainly adopts the maximum stress of 1×10^7 without damage as the fatigue limit. In order to meet the development requirements of high reliability and long life of aero-engine, this work took the maximum stress of 3×10^7 without damage as the fatigue limit. The high-cycle fatigue properties at different temperatures were studied, the effect of stress concentration factor on the fatigue limit at different temperatures was analyzed, and the fracture characteristics of the fatigue specimens were analyzed.

2 Material and Experimental Procedures

2.1 Materials

The material used in this study was industrial ingot of TC4 alloy, which was melted through triple VAR melting, then processed into Φ 30 mm bar in $\alpha + \beta$ region by precision forging. The bar of equal length was cut and forged in $\alpha + \beta$ region to prepare a 60 × 40 × 15 mm flattened sample. The sample was subjected to ordinary annealing heat treatment at 700 °C for 2 h following by air cooling. The basic tensile properties obtained are shown in Table 1.

Table 1. Tensile properties tested at different temperatures for TC4 titanium alloy specimens.

T/°C	R_m/MPa	$R_{p0.2}$/MPa	A/%	Z/%
RT	1030	943	16.6	44.0
100	950	829	20.8	50.5
200	861	728	19.8	59.1
300	780	648	17.5	60.9
400	747	614	17.6	62.9

2.2 Experimental Procedures

Samples were taken along the longitudinal direction of the flattened sample and processed into the fatigue test sample shown in Fig. 1. The fatigue test was conducted on the QBWP type rotary bending fatigue testing machine, and the test preparation and process were strictly in accordance with the ISO 1143: 2010 metallic materials-rotating bar bending fatigue standard. In the air environment, the test temperatures were room temperature, 200 °C and 400 °C respectively, the stress concentration factor was $K_t = 1$ and $K_t = 3$, and the test speed was 5000r/min. The fatigue limit under the specified life of 3×10^7 was obtained by the lifting method, and each set of data met the 95% confidence requirement under the 50% survival rate.

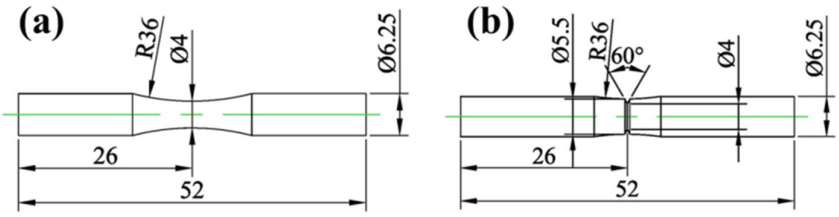

Fig. 1. Schematic diagram of high cycle fatigue **a** smooth and **b** notch specimens.

The fatigue fracture morphology and the microstructure of the samples were observed by JSM-7900F field emission scanning electron microscope (SEM) equipped with electron back-scattered diffraction (EBSD) detector. The diameter-axial surface of the sample was selected, and the microstructure characteristics were observed by SEM after mechanical polishing and chemical etching. The proportion of etching solution was 5 vol.%HF + 10vol.%HNO_3 + 85vol.%H_2O. The EBSD samples were prepared by electrolytic polishing with a mixed solution of 6% perchloric acid, 35 vol.% n-butanol and 59 vol.% methanol. The temperature of the polishing solution was controlled to about −25 °C and the voltage was about 20 V. The scanning area was 245 μm × 190 μm with a step size of 0.4 μm.

3 Results and Discussion

3.1 Microstructure

The microstructure of the TC4 alloy sample is shown in Fig. 2. It can be seen that after annealing, the TC4 alloy has a typical bi-modal structure, which is mainly composed of ellipsoid primary α phase and lath secondary α phase, and β phase is distributed among the secondary α phases. The content of primary α phase is about 40%, and the size is 5–15 μm (Fig. 2a). The crystal orientation distribution of the sample was obtained by EBSD analysis (Fig. 2b). It can be seen that the grain orientation of the primary α-phase is similar, and the grain orientation difference of the secondary α-phase varies greatly in comparison. Figure 2c is the pole figure corresponding to the orientation distribution. The relatively concentrated crystal orientations were <0001>//RD and <10 $\bar{1}$ 0>//RD

(ie, the sampling direction) deformation texture, which indicates that the sample still retains the texture formed by precision forging after flattening and annealing. However, the texture density was relatively low, and the maximum texture strength was 4.389.

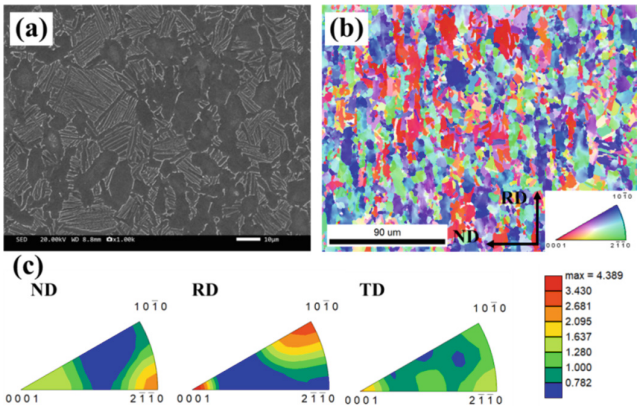

Fig. 2. Microstructure of TC4 alloy **a** SEM morphology; **b** inverse pole figure; **c** inverse pole figures parallel to ND, TD and RD.

3.2 High Cycle Fatigue Properties

The stress fatigue life curve (*S-N* curve) is the fatigue life curve measured under the condition that the maximum cyclic stress does not exceed the elastic limit or yield strength, and is one of the main basis for evaluating the fatigue performance of materials. Generally, there are three expressions of *S-N* curve, the power function expression, the exponential function expression and the three-parameter power function expression [15]. The three-parameter power function method was used to fit the rotational bending fatigue *S-N* curves of the smooth ($K_t = 1$) and notched ($K_t = 3$) specimens of the TC4 alloy at different temperatures, as shown in Fig. 3. It can be seen that with the increase of the test temperature, the fatigue life shows a downward trend, indicating that the temperature has a significant effect on the fatigue properties of the TC4 alloy. This is related to the change of the deformation mechanism of the material at high temperature. The resistance to crack initiation and propagation decreases at high temperature [16–18]. Comparing the fatigue curves with different stress concentration factors, it can be seen that for the smooth specimen, the fatigue performance is more sensitive to the change of temperature. The *S-N* (median value) fatigue curve equation and corresponding fatigue limit of TC4 alloy under different test conditions are shown in Table 2. It can be seen that under the same test conditions, the fatigue life of the notched specimens is significantly reduced, which is consistent with previous investigation [19]. Compared with the smooth specimens, the fatigue limit(σ_D) of the notched specimens is reduced by 65.6, 65.7 and 64.9% at room temperature, 200 °C and 400 °C, respectively, indicating that the high-cycle fatigue properties of TC4 alloys exhibit obvious notch-sensitive effects at room temperature and high temperature.

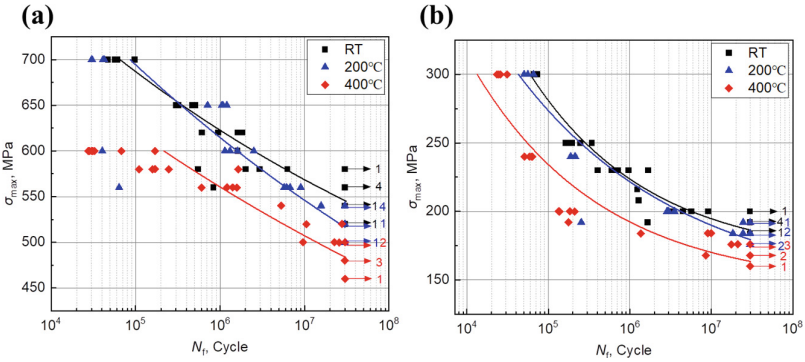

Fig. 3. *S-N* curves of TC4 alloy **a** smooth and **b** notched samples at different temperatures.

Table 2. Fatigue limit and S-N equation of TC4 alloy under different conditions.

Stress concentration	Temperature/°C	S-N equation	σ_D/MPa
$K_t = 1$	RT	$\lg N_f = 40.54–13.59\lg(\sigma_{max}-275)$	570
	200	$\lg N_f = 47.53–15.41\lg(\sigma_{max}-120)$	542
	400	$\lg N_f = 55.76–18.69\lg(\sigma_{max}-100)$	498
$K_t = 3$	RT	$\lg N_f = 11.98–3.38\lg(\sigma_{max}-165)$	196
	200	$\lg N_f = 14.95–4.68\lg(\sigma_{max}-140)$	186
	400	$\lg N_f = 12.10–3.64\lg(\sigma_{max}-145)$	175

3.3 High Cycle Fatigue Properties

Figure 4 shows the fatigue fracture morphologies of the smooth specimen at room temperature and 400 °C. It can be clearly seen that the fatigue fracture is divided into three typical regions, the fatigue crack source region, the crack propagation region and the instantaneous fracture region. Since the experiment adopts a rotating bending loading method, leading to the surface of the sample is subjected to a large stress, the crack source is usually formed on the surface or subsurface [20]. At room temperature, the crack of the smooth specimen started on the surface, with only one crack source area, accompanied by an obvious radial pattern (Fig. 4b). The crack propagation rate in this area is slow, and the cracks are repeatedly opened and closed under cyclic loads, causing friction on the surface, therefore they are generally flat and smooth. As the crack propagates into the crack propagation region, a large area of dense fatigue stripes can be seen, accompanied by a small number of secondary cracks (Fig. 4c). Fatigue stripes will increase the non-uniform deformation during crack propagation and hinder crack growth. The thinner the fatigue strip, the greater the resistance of the material to crack growth and the slower the crack propagation [21]. The instantaneous fracture region is composed of many small dimples, showing typical ductile fracture characteristics (Fig. 4d). However, at 400 °C, the cracks of the smooth specimens start from the interior of the specimens,

which is also the origin of single-source cracks. Due to the weak resistance to crack propagation at high temperature, the crack source region is flatter, and the fatigue band in the propagation region is slightly wider than that at room temperature. As the crack propagates, an instantaneous fracture occurs on the inner side of the opposite side of the crack source area after instability occurs, forming a larger dimple.

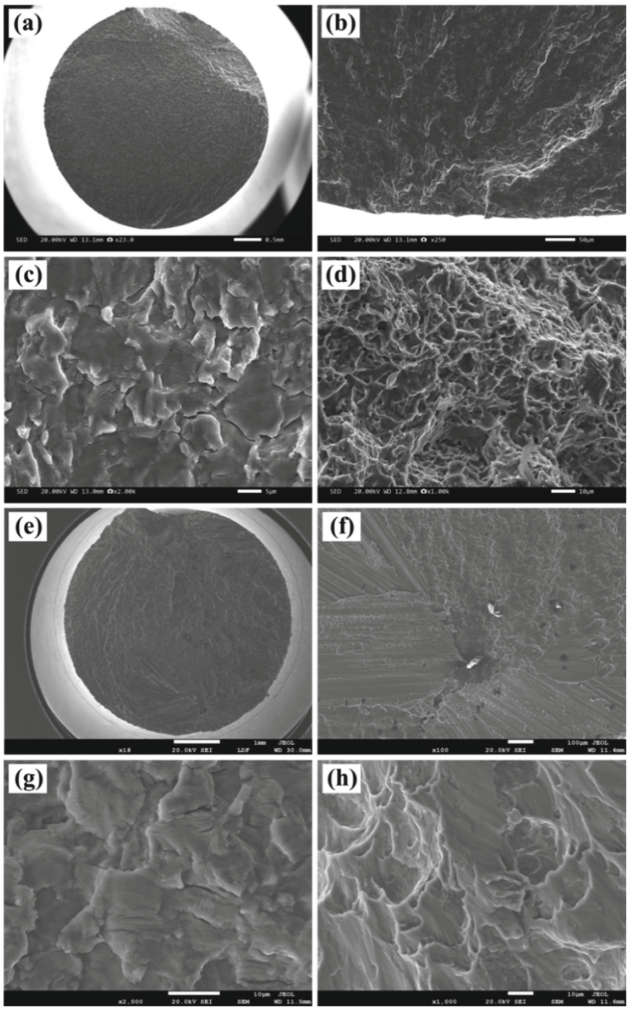

Fig. 4. Fatigue fracture morphology of TC4 alloy smooth specimens at room temperature (σ = 580 MPa, $N_f = 2.96 \times 10^6$): **a** macroscopic micrograph, **b** fatigue crack initial stage, **c** region of stable crack growth, **d** fast fracture zone; and 400 °C (σ = 500 MPa, $N_f = 2.57 \times 10^7$): **e** macroscopic micrograph, **f** fatigue crack initial stage, **g** region of stable crack growth, **h** fast fracture zone.

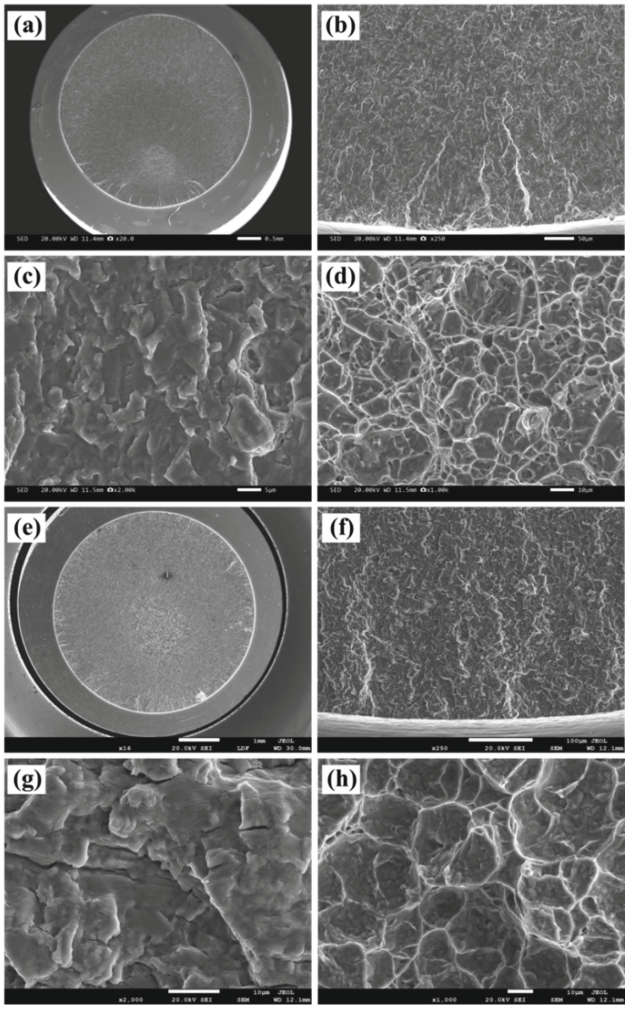

Fig. 5. Fatigue fracture morphology of TC4 alloy notched specimens at room temperature (σ = 200 MPa, $N_f = 9.19 \times 10^6$): **a** macroscopic micrograph, **b** fatigue crack initial stage, **c** region of stable crack growth, **d** fast fracture zone; and 400 °C (σ = 176 MPa, $N_f = 2.11 \times 10^7$): **e** macroscopic micrograph, **f** fatigue crack initial stage, **g** region of stable crack growth, **h** fast fracture zone.

Figure 5 shows the fatigue fracture morphologies of the notched specimens at room temperature and 400 °C. Different from the smooth specimens, the notched specimens exhibited multiple crack sources on the surface at both room temperature and high temperature. This is attributed to the stress concentration at the root of the notch is the largest in the process of fatigue loading. Fatigue failure starts in weak areas where stress concentrations are concentrated, resulting in a significant decrease in fatigue performance. With the crack propagation, obvious fatigue strips can also be observed in the

steady-state propagation region, and more secondary cracks can be seen in the fatigue propagation region at high temperature. Unlike the smooth specimen, the fatigue crack of the notched specimen propagates inward from the circumference, and finally an instantaneous fracture occurs in a small area inside the specimen, which exhibits ductile fracture characteristics.

4 Conclusions

(1) The *S-N* curves of smooth and notched specimens of TC4 alloy were measured at room temperature, 200 °C and 400 °C. The high cycle fatigue of TC4 alloy shows obvious notch sensitive effect at room and high temperature. When $N_f = 3 \times 10^7$ cycles, the fatigue limits of smooth specimens are 574 MPa, 542 MPa and 543 MPa respectively, and the fatigue limits of notched specimens are 196MPa, 186MPa and 175MPa, respectively.

(2) With the increase of temperature, the high cycle fatigue properties of TC4 alloy were decreased. For the smooth specimen with $K_t = 1$, the effect of temperature on fatigue performance was more obvious.

(3) Both of room temperature and high temperature smooth samples had only one fatigue crack source. The room temperature fatigue crack originated from the surface of the smooth specimen, while the high temperature fatigue crack originated from the interior of the specimen. Obvious fatigue strips and a few secondary cracks can be seen in the propagation zone. With the crack propagation, instantaneous fracture occurred in the opposite and inner side of the crack source region, which was characterized by ductile fracture.

(4) Fatigue cracks of notched specimens originated in the notched root region with large stress concentration, and there were multiple fatigue crack sources. Fatigue bands can be seen in the propagation zone, accompanied by more secondary cracks at high temperature. The fatigue cracks extended from the circumference inward, and finally occurred instantaneous fracture in a small area inside the sample.

References

1. Banerjee, D., Williams, J.: Perspectives on titanium science and technology. Acta Mater. **61**(3), 844–879 (2013)
2. Leyens, C., Peters, M.: Titanium and Titanium Alloys: Fundamentals and Applications. Wiley (2003)
3. Cui, C., Hu, B., Zhao, L., et al.: Titanium alloy production technology, market prospects and industry development. Mater. Des. **32**(3), 1684–1691 (2011)
4. Seshacharyulu, T., Medeiros, S.C., Frazier, W.G., et al.: Hot working of commercial Ti-6Al-4V with an equiaxed α−β microstructure: materials modeling considerations. Mater. Sci. Eng. **284**(1–2), 184–194
5. Wang, X.D., Hao, B., Lu, F.S., et al.: The basic properties and application situation of titanium in China. Titan. Ind. Prog. **21**(1), 6–10 (2004)
6. Cheng, M., Zhao, J.G., Song, H.W., et al.: Effect of α grain size on deformation behaviors of TC4 titanium alloy with equiaxed microstructure. J. Aeronaut. Mater. **29**(1), 22–26 (2009)

7. Lütjering, G.: Influence of processing on microstructure and mechanical properties of (α+ β) titanium alloys. Mater. Sci. Eng. **243**(1–2), 32–45 (1998)
8. Evans, W.: Optimising mechanical properties in alpha + beta titanium alloys. Mater. Sci. Eng. **243**(1–2), 89–96 (1998)
9. Tao, C.H., Liu, Q.Q., Cao, C.X.: Failure and Prevention of Aeronautical Titanium Alloy, p. 39. National Defence Industry Press, Beijing (2002)
10. Zhong, P.D.: Failure and lesson of turbo rotation blades of aero-engines. J. Mater. Eng. **31**(z1), 30–33 (2003)
11. Cowles, B.A.: High cycle fatigue in aircraft gas turbines-an industry perspective. Int. J. Fract. **80**(2/3), 147–163 (1989)
12. Tokaji, K., Mito, N.: High cycle fatigue behaviour of Ti-6Al-4V alloy at elevated temperatures. Scripta Mater. **54**(12), 2143–2148 (2006)
13. Nalla, R.K., Boyce, B.L., Campbell, J.P., et al.: Influence of microstructure on high-cycle fatigue of Ti-6Al-4V: bimodal versus lamellar structures. Metall. Mater. Trans. **33**(13), 899–918 (2002)
14. Li, J., Cai, J.M., Duan, R., et al.: High cycle fatigue of TC6 alloy. **23**(z1), s277–s281 (2013)
15. Li, Y., Zhang, C.C., Gao, J.Y., et al.: High-cycle and giga-cycle fatigue properties of titanium alloy for aero-engine. Mech. Eng. **38**(3), 250–254 (2016)
16. Li, J.K., Liu, Y.J., Wang, Q.Y., et al.: High-temperature ultra-high cycle fatigue test of TC17 titanium alloy. Hangkong Dongli Xuebao/J. Aerosp. Power **29**(7), 1567–1573 (2014)
17. Li, G., Sun, C.Q.: High-temperature failure mechanism and defect sensitivity of TC17 titanium alloy in high cycle fatigue. J. Mater. Sci. Technol. **122**, 128–140 (2022)
18. Chen, Y.N., Xiong, Y., Fan, M.X., et al.: Fatigue facture analysis of TC11 titanium alloy at different temperatures. Trans. Mater. Heat Treat. **8**, 8 (2019)
19. Liu, Y., Le, Z., Shi, X., et al.: High cycle fatigue properties and fracture behavior of Ti–5Al–5Mo–5V–1Cr–1Fe titanium alloy. Rare Met. Mater. Eng. **47**(12), 3666–3671 (2018)
20. Sun, Y.L., Yu, J.J., Wang, Z.J., et al.: Rotary bending high cycle fatigue behavior of single crystal superalloy DD499 in <111> orientation. Rare Met. Mater. Eng. **40**(2), 239–242 (2011)
21. Morrissey, R.J., Mcdowell, D.L., Nichloas, T.: Frequency and stress ratio effects in high cycle fatigue of Ti-6Al-4V. Int. J. Fatigue **21**(7), 679–685 (1999)